Inorganic Chemistry

Article

pubs.acs.org/IC

Integrated and Passive 1,2,3-Triazolyl Groups in Fluorescent Indicators for Zinc(II) Ions: Thermodynamic and Kinetic Evaluations

J. Tyler Simmons,[†] John R. Allen,[‡] Deborah R. Morris,[§] Ronald J. Clark,[†] Cathy W. Levenson,*[,§] Michael W. Davidson,*[,‡] and Lei Zhu*[,†]

[†]Department of Chemistry and Biochemistry, Florida State University, 95 Chieftan Way, Tallahassee, Florida 32306-4390, United States

[‡]National High Magnetic Field Laboratory and Department of Biological Science, Florida State University, 1800 East Paul Dirac Drive, Tallahassee, Florida 32310, United States

[§]Department of Biomedical Sciences, College of Medicine, Florida State University, 1115 W. Call Street, Tallahassee, Florida 32306-4300, United States

Supporting Information

ABSTRACT: In addition to being a covalent linker in molecular conjugation chemistry, the function of a 1,2,3-triazolyl moiety resulting from the copper(I)-catalyzed azide−alkyne cycloaddition reaction as a ligand for metal ions is receiving considerable attention. In this work, we characterize the thermodynamic and kinetic effects of incorporating a 1,2,3-triazolyl group in a multidentate ligand scaffold on metal coordination in the context of fluorescent zinc(II) indicator development. Ligands **L14**, **BrL14**, and **FL14** (1,4-isomers) contain the 1,4-disubstituted-1,2,3-triazolyl group that is capable of binding with zinc(II) in conjunction with a di(2-picolylamino) (DPA) moiety within a multidentate ligand scaffold. Therefore, the 1,2,3-triazolyl in the 1,4-isomers is "integrated" in chelation. The 1,5-isomers **L15**, **BrL15**, and **FL15** contain 1,2,3-triazolyls that are excluded from participating in zinc(II) coordination. These 1,2,3-triazolyls are "passive linkers". Zinc(II) complexes of 2:1 (ligand/metal) stoichiometry are identified in solution using ^{1}H NMR spectroscopy and isothermal titration calorimetry (ITC) and, in one case, characterized in the solid state. The 1:1 ligand/zinc(II) affinity ratio of **L14** over **L15**, which is attributed to the affinity enhancement of a 1,2,3-triazolyl group to zinc(II) over that of the solvent acetonitrile, is quantified at 18 (−1.7 kcal/mol at 298 K) using an ITC experiment. Fluorescent ligands **FL14** and **FL15** are evaluated for their potential in zinc(II) sensing applications under pH neutral aqueous conditions. The 1,4-isomer **FL14** binds zinc(II) both stronger and faster than the 1,5-isomer **FL15**. Visualization of free zinc(II) ion distribution in live HeLa cells is achieved using both **FL14** and **FL15**. The superiority of **FL14** in staining endogenous zinc(II) ions in live rat hippocampal slices is evident. In summation, this work is a fundamental study of 1,2,3-triazole coordination chemistry, with a demonstration of its utility in developing fluorescent indicators.

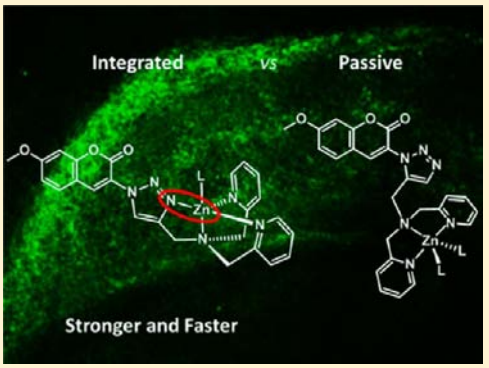

INTRODUCTION

The [3 + 2] cycloaddition of azide and alkyne affords 1,2,3-triazoles,[1] which have recently been utilized in a wide variety of research fields, including catalysis,[2−7] sensing,[8,9] bioconjugation,[10] and magnetic materials development.[11,12] The renaissance of 1,2,3-triazole chemistry is primarily due to the discovery by Fokin, Sharpless,[13] and Meldal[14] of regiospecific synthesis of 1,4-disubstituted-1,2,3-triazoles via the copper(I)-catalyzed azide−alkyne cycloaddition (CuAAC). It was later shown that 1,5-disubstituted-1,2,3-triazoles can be prepared also regioselectively, using Ru- or base-catalyzed approaches (Scheme 1).[15−18]

The 1,2,3-triazolyl moiety resulting from the CuAAC reaction has been used primarily as a passive covalent linker in bridging together two molecular components. More recently, the functionality of 1,2,3-triazole itself has been appreciated, in

Scheme 1. Three Approaches to the Syntheses of 1,2,3-Triazoles via Azide−Alkyne Cycloaddition

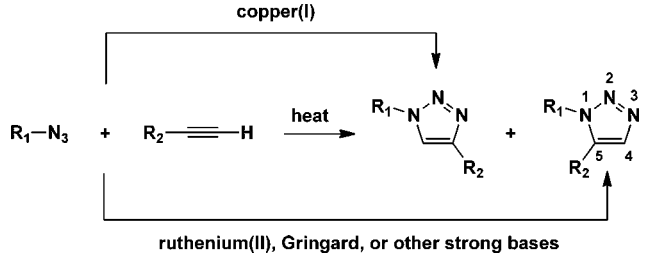

Received: December 19, 2012
Published: April 26, 2013

   dx.doi.org/10.1021/ic302798u | Inorg. Chem. 2013, 52, 5838−5850

particular as a metal coordination ligand.[19−21] To this end, the ability of a 1,2,3-triazole to act as integrated components in multidentate ligand scaffolds (e.g., see Figure 1, left[22]) has

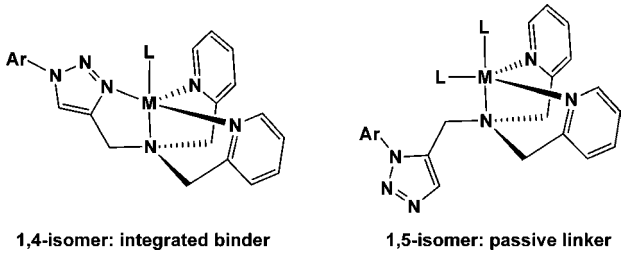

Figure 1. 1,2,3-Triazolyl group assists in metal (M) coordination (left), or acts only as a covalent linkage (right) between the aryl (Ar) group and the metal coordination site in 1,4- and 1,5-isomeric ligands, respectively. Symbol "L" denotes a monodentate ligand or solvent.

begun to receive considerable attention. With the increasing role of 1,2,3-triazolyl moiety in coordination chemistry, a quantitative analysis of the thermodynamic and kinetic benefits of incorporating a 1,2,3-triazolyl group in a multidentate ligand would be valuable to the future designs of 1,2,3-triazolyl-containing ligands. Herein, we report such a study that was undertaken in the context of developing fluorescent indicators for zinc(II) ions.

Zinc(II) ion is known to be a key regulator of several important biological processes.[23−25] Because of the lack of spectroscopic signature of zinc(II) ions, the use of a zinc(II)-reporting fluorescent indicator under physiological conditions has become the method of choice for detecting and tracking zinc(II) ions in cell- and neuro-biological experiments.[26] Ideally, zinc(II) indicators undergo a significant change in either fluorescence intensity and/or frequency upon zinc(II) binding. Other desirable properties of a zinc(II) indicator include facile synthesis, visible light excitation, high water solubility, tunable affinity for zinc(II) via convenient ligand modification, fast but reversible binding kinetics, photostability, and high brightness.[26,27] Reflecting the extensive activities in the pursuit of suitable zinc(II) indicators in various applications, numerous reviews have been published on this topic over the past decade.[26,28−37]

1,2,3-Triazolyl-containing compounds **1**−**3** have been developed as fluorescent indicators for zinc(II) ions (see Chart 1). In these compounds, the 1,2,3-triazolyl group acts as both a ligand for helping chelate zinc(II) ion and a linker to join a fluorophore and the coordination site, which constitutes an integrated design.[19] Our group reported compound **1**, which includes an anthryl fluorophore and a 1,2,3-triazolyl-containing acyclic tetradentate ligand.[22a,38] Compound **1** shows potential in imaging zinc(II) distribution in live mammalian cells.[38] However, the moderate brightness of the zinc(II) complex ($\varepsilon \times \phi_F$ = 711 at an excitation wavelength of 300 nm) and high energy excitation of the anthryl fluorophore limit the utility of this compound in bioimaging experiments. Watkinson and Todd showed that a 1,2,3-triazolyl group acts as an integrated binder for zinc(II) ions in their cyclam-based sensors (e.g., compound **2**).[39,40] The visualization of zinc(II) in zebrafish embryos was accomplished in their work. In another notable study, Belfield and co-workers developed compound **3** as a two-photon excited probe for zinc(II).[41a] Finally, a zinc(II) sensor that applied only 1,2,3-triazolyl groups for coordination was reported recently.[41b]

In the current study, the properties that we seek to improve upon, relative to the previous contributions, are the inherent brightness ($\varepsilon_{ZnL} \times \phi_{ZnL}$) and the fluorescence contrast between free- and zinc(II)-bound forms (ϕ_{ZnL}/ϕ_L) of 1,2,3-triazolyl-containing indicators under pH neutral aqueous conditions. Furthermore, by comparing isomeric 1,2,3-triazolyl-containing ligands (Figure 1), in which the 1,2,3-triazolyl group is either an "integrated binder" (1,4-isomer on the left) or a "passive linker" (1,5-isomer on the right), the thermodynamic and kinetic contributions of the 1,2,3-triazolyl group to zinc(II) coordination are deduced.

RESULTS AND DISCUSSION

Experimental Design. The zinc(II) coordination chemistry of both 1,4- (**L14** or **BrL14**) and 1,5-isomers (**L15** or **BrL15**) were studied in CH_3CN using isothermal titration calorimetry (ITC) and ^1H NMR spectroscopy. (See Chart 2.)

Chart 2. Structures of 1,4- and 1,5-Isomeric Ligands

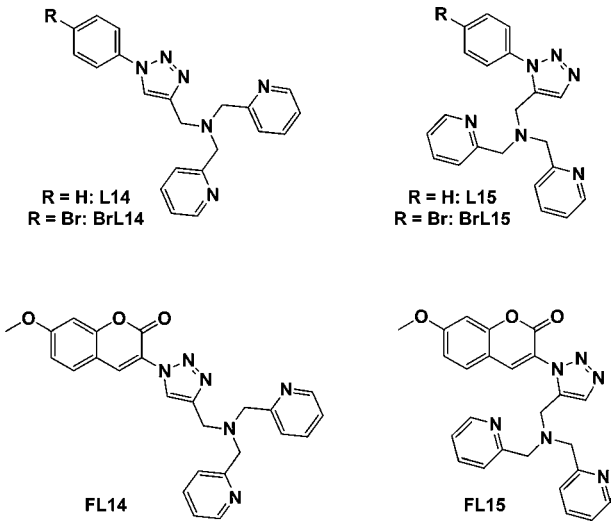

These ligands are easier to prepare in large quantities than the fluorescent analogs **FL14** and **FL15**. Therefore, they were used

Chart 1. Fluorescent Zinc(II) Indicators That Integrate 1,2,3-Triazolyl Groups

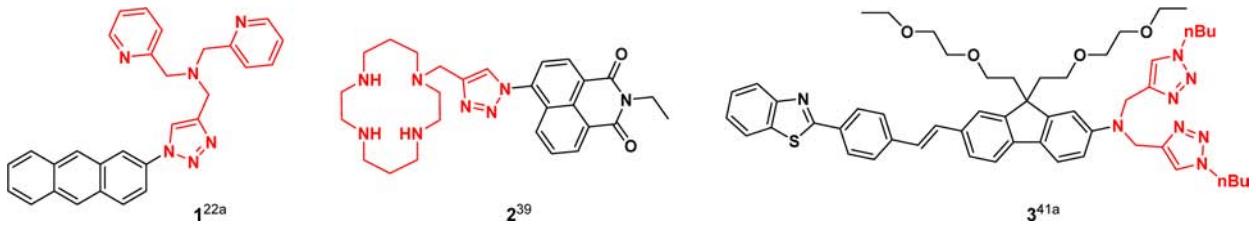

dx.doi.org/10.1021/ic302798u | Inorg. Chem. 2013, 52, 5838−5850

to complete the concentration-demanding ITC and ^{1}H NMR experiments. The brominated ligands **BrL14** and **BrL15** carry the benefit of an enhanced propensity to crystallize, which aids in the acquisition of single-crystal structures of the zinc(II) complexes. From ITC, all thermodynamic parameters of a ligand/receptor equilibrium ($\Delta G°$, $\Delta H°$, and $\Delta S°$) can be obtained,[42] and the difference in binding affinities associated with 1,2,3-triazolyl binding can be quantified. Fluorescent ligands **FL14** and **FL15** were investigated as potential fluorescent indicators for zinc(II) ions. Zinc(II)-dependent fluorescence of ligands **FL14** and **FL15** was studied under pH neutral aqueous conditions. Competitive binding experiments were used to compare their affinities for zinc(II). Stopped-flow kinetic measurements were conducted to determine the second-order rate constants k_{on} of both isomers. The viability of **FL14** and **FL15** as fluorescent zinc(II) indicators in imaging zinc(II) ions in both mammalian cells and rat hippocampal slices was demonstrated.

Synthesis. **L14** was synthesized from azidobenzene and *N*,*N*-di(2-picolyl)propargylamine via a CuAAC reaction in 60% yield (Scheme 2) as reported earlier.[22a] **L15** was prepared in

Scheme 2. Reagents and Conditions: (a) $Cu(OAc)_2·H_2O$ (5 mol %), Sodium Ascorbate (25 mol %), CH_3OH, rt, 20 h, 60%; (b) toluene, 70 °C, 12 h, 89%; (c) PBr_3, CH_2Cl_2, rt, 6 h, 49%; (d) DIPEA, $CHCl_3$, rt, 16 h, 95%

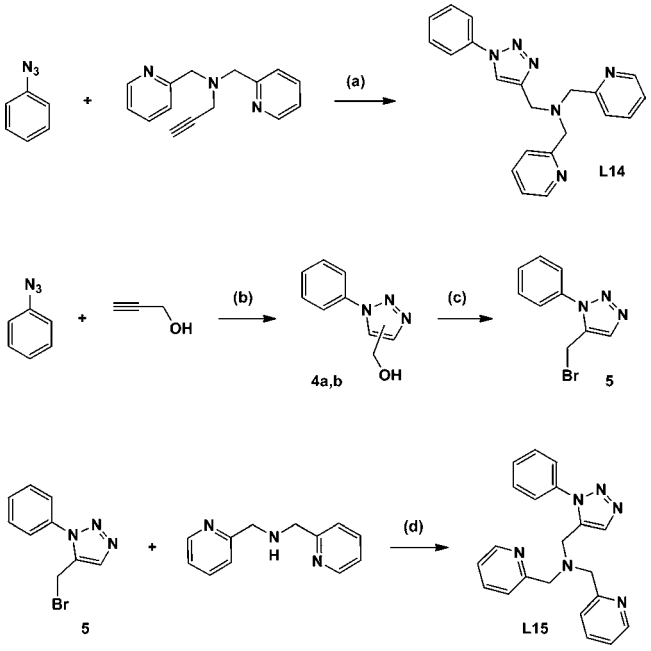

three steps, starting with the thermal 1,3-dipolar cycloaddition of azidobenzene and propargyl alcohol to give a mixture of the 1,4- and 1,5-triazole isomers, **4a** and **4b**, with 89% total conversion from azidobenzene. The ruthenium(II)-catalyzed procedure to give 1,5-disubstituted-1,2,3-triazoles[17,43] also could be used. However, aromatic azides have low reactivities under these conditions.[17] Because of the low cost of the starting materials, high product conversion, and ease of separation of the regioisomers in a later step, the thermal cycloaddition method was used in the current work. Bromination of the mixture of **4a** and **4b** with PBr_3, followed by chromatographic separation, gave the 1,5-isomer **5** in 49% yield (from the mixture of **4a** and **4b**). Finally, S_N2 substitution with di(2-picolyl)amine yielded **L15** in 95%. Other ligands were synthesized in a similar fashion starting from 1-azido-4-bromobenzene (**BrL14** and **BrL15**; see Scheme S6 in the Supporting Information) or 3-azido-7-methoxycoumarin (**FL14** and **FL15**; see Schemes S7 and S8 in the Supporting Information).

Solid-State Structures. Single crystals of formula $[Zn(\mathbf{BrL14})(CH_3CN)](ClO_4)_2$ and $[Zn(\mathbf{L15})(H_2O)]_n(ClO_4)_{2n}$ (Figure 2) were obtained from vapor diffusion of diethyl ether into CH_3CN solutions of the complexes. The distances of coordinative bonds are shown in the caption of Figure 2. Similar to our previously reported 1,4-isomer/zinc(II) complexes,[22,38] the structure of $[Zn(\mathbf{BrL14})(CH_3CN)](ClO_4)_2$ contains a distorted trigonal bipyramidal zinc(II) center that is bound with the N3 position of the 1,2,3-triazolyl group (Figure 2B). The trigonal bipyramidal core of $[Zn(\mathbf{L15})(H_2O)]_n(ClO_4)_{2n}$ also consists of two pyridyl groups and a 1,2,3-triazolyl group (from a different molecule) on the trigonal plane, while the axial positions are occupied by the tertiary amino group and a H_2O molecule (Figure 2D). The incorporation of a 1,2,3-triazolyl group from a nearby ligand allows for the formation of a polymeric chain (Figure 2E).

The single crystals of the 2:1 (ligand/metal) complex between **BrL15** and zinc(II) were afforded using the same vapor diffusion approach. The bond distances in the zinc(II) coordination sphere are shown in the caption of Figure 3. A *fac* isomer of C_2 symmetry was observed (Figure 3), in which the two 2-pyridylmethyl groups in the same molecule are no longer equivalent. This feature is also seen in the ^{1}H NMR spectrum of the 2:1 complex in solution (vide infra). The 2:1 (ligand/zinc(II)) octahedral complexes involving two *N*,*N*-di(2-picolyl)amino (DPA) tridentate ligands are relatively rare.[46−49] Despite the difference in the *N*-substituent of the DPA ligands, all but one[46] of the reported cases share the same *fac*/C_2-symmetric stereoisomer, suggesting a thermodynamic preference for its formation.

Characterization of Zinc(II) Coordination in CH_3CN. Isothermal titration calorimetry (ITC) is a valuable tool for investigating the thermodynamics of small molecule/metal coordination systems.[12,38,50−55] We developed an experimental procedure based in Scheme 3 that allows one to determine the affinity of N3 of 1,2,3-triazolyl group (see the numbering in Scheme 3A) to zinc(II), which accounts for the difference in zinc(II) affinities of **L14** and **L15**.

With **L14**, we envision a sequence of binding events where a 1:1 complex would form first as **L14** is titrated into a solution of $Zn(ClO_4)_2$. The 1:1 complex is shown as [Zn(L)(T)(S)] in Scheme 3A, in which L, T, and S represent *N*,*N*-di(2-picolyl)amino, 1,2,3-triazolyl, and CH_3CN, respectively. The 1,4-isomer **L14** would allow for incorporation of the 1,2,3-triazolyl group (T) into the coordination sphere of the 1:1 complex (Scheme 3A). Therefore, L, T, and S are all bound with zinc(II). The ITC data in Figure 4A confirms the initial formation of a 1:1 complex. The binding affinity of this complex (K_1) is too strong to be accurately determined (Scheme 4A).[56] Upon further addition of **L14** in the system, the 2:1 ligand/metal complex ($[Zn(L)_2](T)_2$ in Scheme 3A) forms with a K_2 value of $(4.0 \pm 0.48) \times 10^4$ M^{-1} (Scheme 4B). The two tridentate *N*,*N*-di(2-picolyl)amino groups likely saturate the octahedral coordination sphere of zinc(II), leaving the 1,2,3-triazolyl unbound. This scenario, as depicted in Scheme 3A, is consistent with the ^{1}H NMR titration data (vide infra).

dx.doi.org/10.1021/ic302798u | *Inorg. Chem.* 2013, 52, 5838−5850

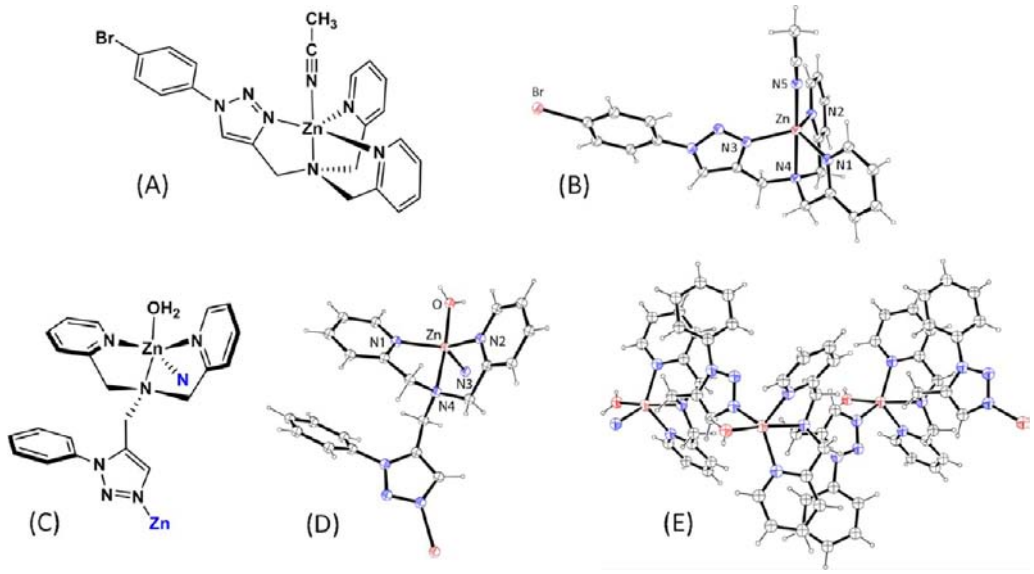

Figure 2. (A) ChemDraw[44] structure and (B) ORTEP[45] diagram of $[Zn(\mathbf{BrL14})(CH_3CN)](ClO_4)_2$ (30% ellipsoids). Selected distances: N1−Zn = 2.035(5) Å; N2−Zn = 2.038(5) Å; N3−Zn = 2.025(5) Å; N4−Zn = 2.233(5) Å; N5−Zn = 2.056(6) Å. (C) ChemDraw[44] structure and (D) ORTEP[45] diagram of $[Zn(\mathbf{L15})(H_2O)]_n(ClO_4)_{2n}$ (30% ellipsoids). (in panel C, the intermolecular attachments to N and Zn are highlighted in blue.) Selected distances: N1−Zn = 2.035(1) Å; N2−Zn = 2.044(1) Å; N3−Zn = 2.023(2) Å; N4−Zn = 2.228(1) Å; O−Zn = 2.086(2) Å. (E) Extended view of $[Zn(\mathbf{L15})(H_2O)]_n(ClO_4)_{2n}$ showing the coordination polymer chain. Noncoordinating solvent molecules and counterions are omitted for clarity. Black denotes hydrogen and carbon, blue denotes nitrogen, red denotes oxygen, and brown indicates zinc.

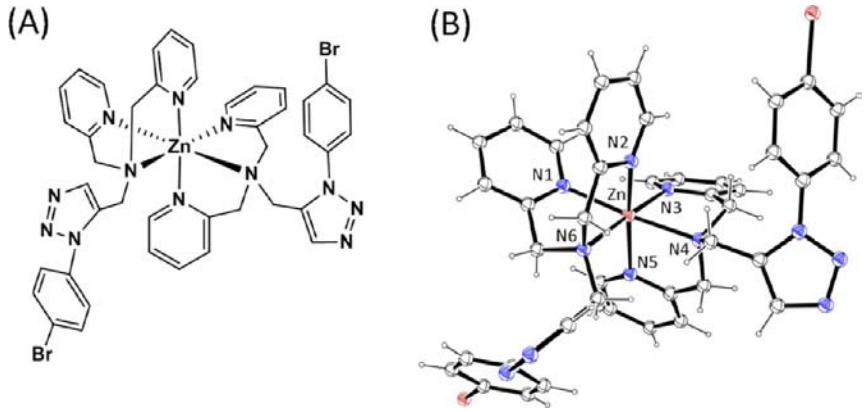

Figure 3. The cationic part of the (A) ChemDraw[44] structure and (B) ORTEP[45] diagram of $[Zn(\mathbf{BrL15})_2](ClO_4)_2$ (30% ellipsoids). Selected distances: N1−Zn = 2.171(2) Å; N2−Zn = 2.105(2) Å; N3−Zn = 2.171(2) Å; N4−Zn = 2.247(2) Å; N5−Zn = 2.105(2) Å; N6−Zn = 2.247(2) Å. Black represents hydrogen and carbon, blue denotes nitrogen, and brown indicates zinc.

The ITC trace of the titration of **L15** into $Zn(ClO_4)_2$ (Figure 4B) at the initial stage is similar to that of **L14**, even though the 1,2,3-triazolyl is not coordinating in the 1:1 complex ($[Zn(L)(S)_2](T)$ in Scheme 3B). The 1:1 binding constant K_3 is also too large to accurately measure (Scheme 4C). The equilibrium constant K_4 (Scheme 4D) of the reaction from the 1:1 complex to the 2:1 complex of **L15** is $(7.0 \pm 0.7) \times 10^5$ M^{-1}, which is over an order of magnitude larger than that of **L14** (K_2 in Scheme 4B). This difference is explained by the affinity lost from the 1,2,3-triazolyl (T) coordination in the 1:1 complex with **L14** ($[Zn(L)(T)(S)]$), which is not present in the 1:1 complex of **L15** ($[Zn(L)(S)_2](T)$). Using Hess's Law, the equilibrium constant of the coordinative exchange between the N3 of the 1,2,3-triazolyl and the solvent molecule CH_3CN to zinc(II) was derived to be 18 (Scheme 4E). This difference appears to largely result from an entropic effect (see $\Delta H°$ and $T\Delta S°$ values in the caption of Figure 4), which suggests that the entropic gain of releasing coordinated solvent molecules accounts for a significant portion of the chelation effect. The coordinative exchange value of 18 (−1.7 kcal/mol at 298 K) can be interpreted as the additional binding affinity of the 1:1 zinc(II) complex of 1,4-isomer **L14**, gained from 1,2,3-triazolyl binding, over that of 1,5-isomer **L15**. Comparing to the zinc(II) affinity gain of 3 orders of magnitude via adding a pyridyl ligand to *N*,*N*-di(2-picolyl)amine to afford *N*,*N*,*N*-tris(2-picolyl)-amine,[57] the effect of a 1,2,3-triazolyl group is rather moderate.

The solution binding properties of **BrL14** and **BrL15** were also studied using ^1H NMR spectroscopy (data of **L14** and **L15** are available in Figures S1 and S2 in the Supporting Information). Upon the addition of $Zn(ClO_4)_2$ to a CD_3CN solution of **BrL14**,[58] peaks associated with the pyridyl protons (peaks "a"−"d" in Figure 5), aliphatic methylene protons (peaks "e" and "f" in Figure 5), and 1,2,3-triazolyl proton (peak "T" in Figure 5) are broadened. The two methylene H_f protons shift upfield from the 2:1 ligand/zinc(II) ratio, similar to the observations made with compound **1**.[38] At a ligand/zinc(II)

dx.doi.org/10.1021/ic302798u | *Inorg. Chem.* 2013, 52, 5838−5850

Scheme 3. Binding Equilibria Envisioned for (A) 1,4-Isomer L14 and (B) 1,5-Isomer upon Titrating Them into a Solution of $Zn(ClO_4)_2$ at 298 K[a]

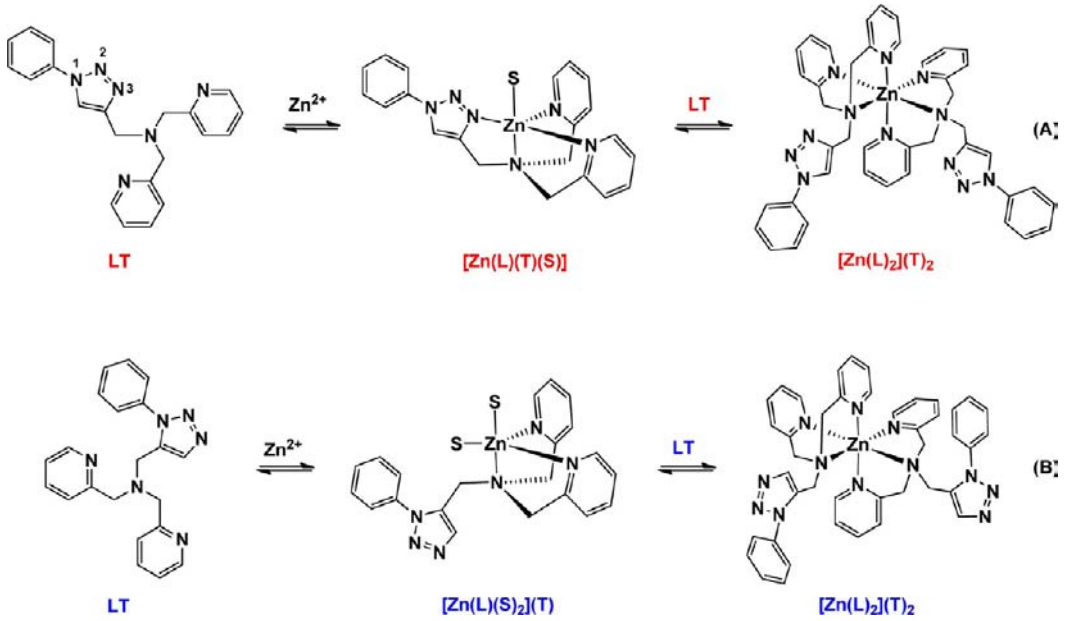

[a]The binding equilibria for the 1,4-isomer is indicated by the red "LT" in panel (A), whereas that for the 1,5-isomer is indicated by the blue "LT" in panel (B). L represents the tridentate *N*,*N*-di(2-picolyl)amino component, T represents the 1,2,3-triazolyl group, and S is the coordinating solvent (in this case, CH_3CN).

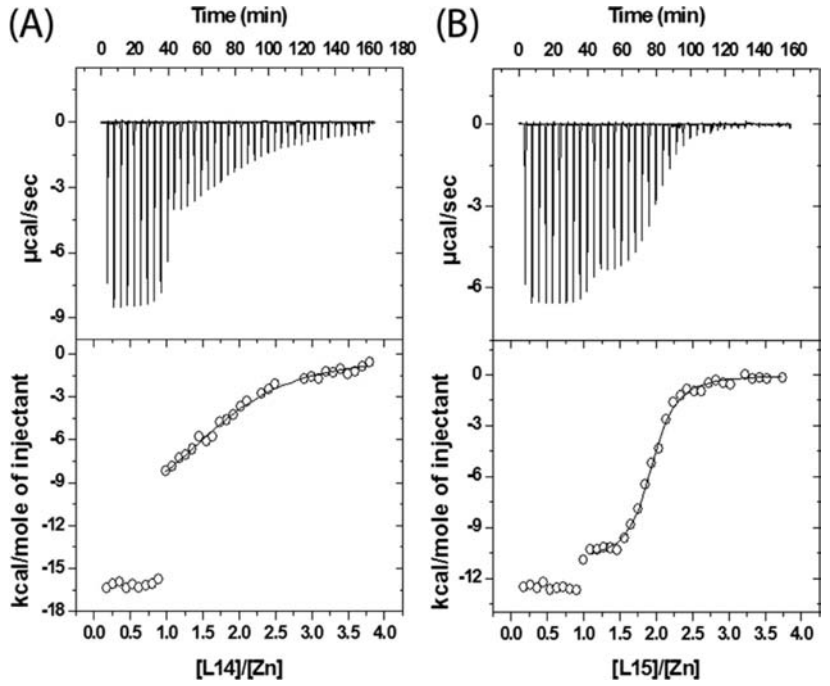

Figure 4. (A) Data for a solution of **L14** (2.0 mM) that was titrated into $Zn(ClO_4)_2$ (0.090 mM) in CH_3CN at 298 K. The one-site model was used to fit the data of the second transition. [Parameters: n (molar ratio) = 1.7 ± 0.07, K = (4.0 ± 0.48) × 10^4 M^{-1}, ΔH = −(12 ± 0.83) kcal/mol, and $T\Delta S°$ = −6.2 kcal/mol.] (B) Data for a solution of **L15** (2.0 mM) that was titrated into a solution of $Zn(ClO_4)_2$ (0.090 mM) in CH_3CN at 298 K. The one-site model was used to fit the data of the second transition. [Parameters: n (molar ratio) = 1.9 ± 0.01, K = (7.0 ± 0.7) × 10^5 M^{-1}, ΔH = −(11 ± 0.02) kcal/mol, and $T\Delta S°$ = −3.0 kcal/mol.]

ratio of 2:1, the pyridyl and aliphatic protons, comparing to 4-phenyl-1,2,3-triazolyl protons, are disproportionally broadened, which is an indication that the *N*,*N*-di(2-picolyl)amino group preferentially binds zinc(II) at the early stage of the titration to form a 2:1 ligand/zinc(II) complex (see structures on the right margin of Figure 5). As the concentration of zinc(II) increases, the peaks resharpen and are shifted downfield. The four methylene protons H_e (Figure 5) are now split into two doublets under the constraints of a five-membered chelating ring with increased kinetic stability, while H_f protons of the

dx.doi.org/10.1021/ic302798u | *Inorg. Chem.* 2013, 52, 5838−5850

Scheme 4. Equilibria Involving L14 (Red Text) and L15 (Blue Text), and the Calculation of the Affinity between the N3 of a 1,2,3-Triazolyl Group with Zinc(II) Ion (Black Text)[a]

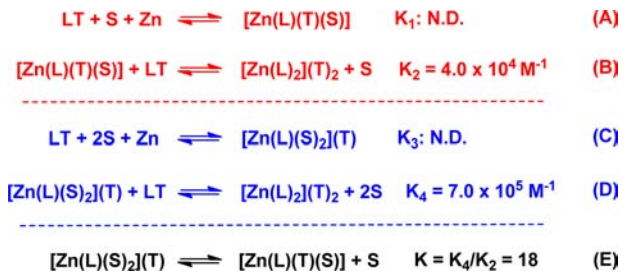

[a]N.D." indicates not determined, because the affinity is higher than the upper limit of the range of determinable values.

1,2,3-triazolyl group remain a singlet. This observation indicates that the dissociation of pyridyl/zinc(II) coordination is slower than that of 1,2,3-triazolyl N3 and zinc(II) ion.[59]

The ^{1}H NMR spectra of **BrL15** collected during the titration experiment (Figure 6) with $Zn(ClO_4)_2$ are strikingly different from that of **BrL14**. Throughout the titration, all peaks remain sharp, and separate sets of peaks can be assigned to species of different coordinated states (i.e., free ligand, 2:1 and 1:1 complexes). This is an indication that the coordination kinetics of the 1,5-isomer, the tridentate ligand **BrL15**, is slower than that of 1,4-isomer tetradendate **BrL14**. It appears that the 2:1 complex of **BrL14** constitutes a shallower minimum on the potential energy surface than that of **BrL15**. The chelatable 1,2,3-triazolyl group in **BrL14** may aid the ligand exchange, i.e., accelerate the equilibrium between the 2:1 and 1:1 complexes.

Early in the titration, two emerging AB systems at 3.4 and 4.3 ppm of two 2-pyridylmethyl groups in **BrL15**, and an apparent singlet (actually a very tight AB system of two diastereotopic 5-(1,2,3-triazolyl)methyl protons; see similar examples in Figures S2 and S8 in the Supporting Information) at 3.2 ppm of equal integrated intensity are assigned to the 2:1 ligand/zinc(II) complex (Figure 6, see the Supporting Information for the rationale of peak assignments). Clearly, the two pyridyl rings in **BrL15** are no longer chemically equivalent in the 2:1 complex. The differentiation of the two pyridyl groups can be taken into account in the 2:1 complex structure depicted in Figure 3, which is a *fac* stereoisomer of C_2 symmetry. The two pyridyl groups of the same ligand are placed in different chemical environments, which are coded red (axial) and blue (equatorial) in the ^{1}H NMR spectrum of the 2:1 complex in Figure 6. Other stereoisomers of the 2:1 complex are possible,[46] but the thermodynamic dominance of the *fac*/C_2 isomer is apparent in the ^{1}H NMR titration experiment. Despite the prevalent use of *N*,*N*-di(2-picolyl)amino group in zinc(II) indicator development and other metal coordination constructs,[60,61] to the best of our knowledge the structural differentiation of the two 2-picolyl groups has not been reported. The 1:1 **BrL15**/zinc(II) complex formed at the end of the titration experiment only shows one set of pyridyl signals, suggesting the return to equivalency of the two pyridyl groups in the 1:1 complex. A singlet and two doublets of an AB system in the aliphatic region are assigned to 5-(1,2,3-triazolyl)methyl H_f and 2-pyridylmethyl H_e, respectively (Figure 6), which is similar to the assignments applied to the 1,4-isomer **BrL14** (Figure 5).

The Viability of FL14 and FL15 as Fluorescent Indicators for Zinc(II) Ions. Fluorescent indicators for

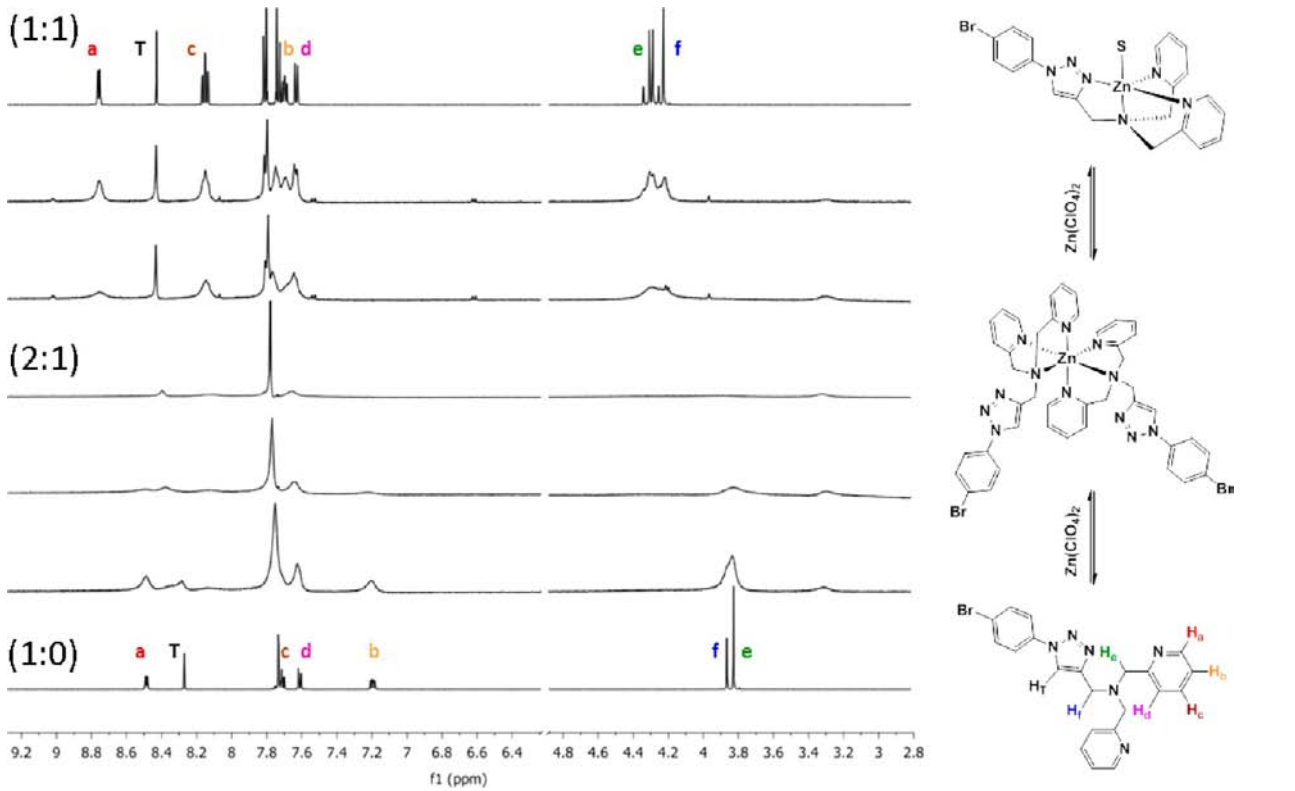

Figure 5. ^{1}H NMR spectra (500 MHz, CH_3CN) of **BrL14** in the presence of increasing concentrations of $Zn(ClO_4)_2$. The assignments are based on 2D-COSY spectra (Figures S3 and S4 in the Supporting Information). S: solvent CD_3CN. Selective ratios of ligand/metal are shown in parentheses.

dx.doi.org/10.1021/ic302798u | Inorg. Chem. 2013, 52, 5838−5850

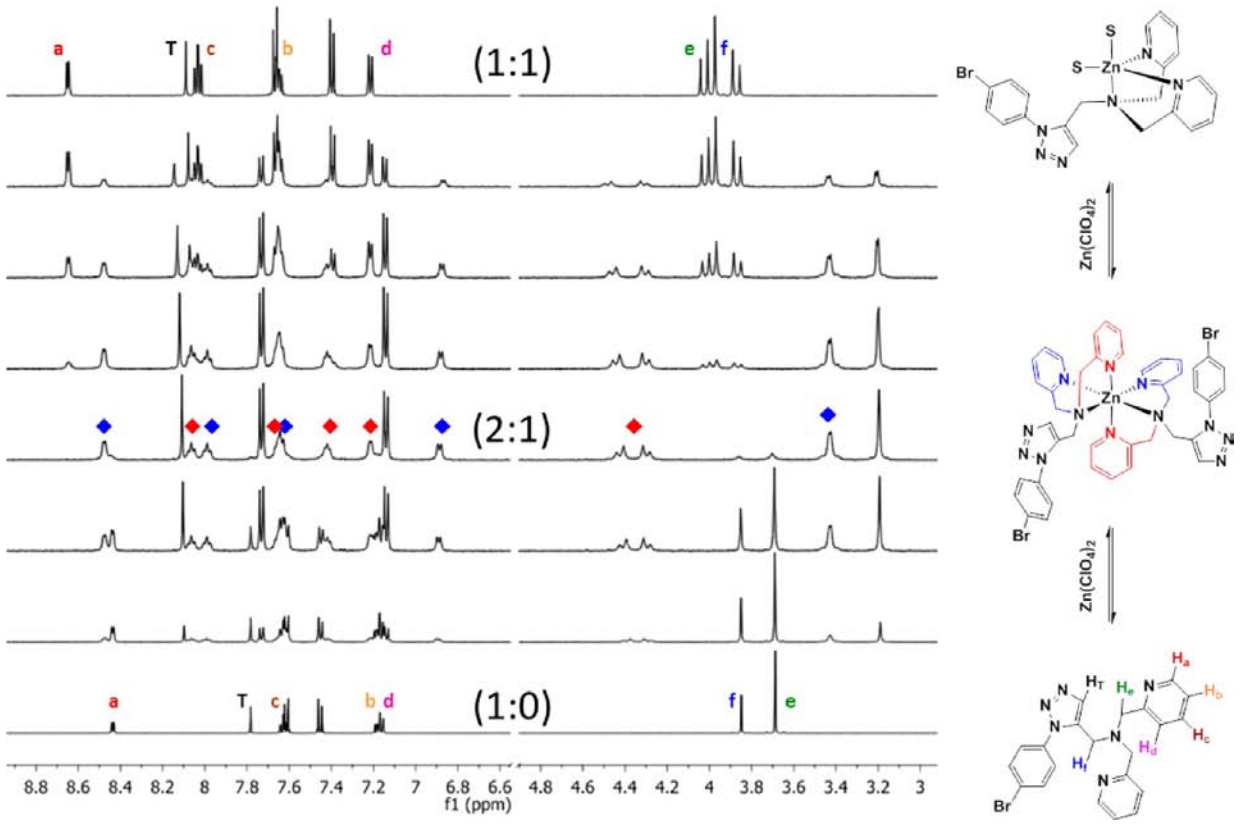

Figure 6. Partial ^{1}H NMR spectra (500 MHz, CD_3CN) of **BrL15** in the presence of increasing concentrations of $Zn(ClO_4)_2$. The assignments are based on 2D-COSY spectra (Figures S5−S7 in the Supporting Information). For the assignment of the 2:1 ligand/zinc(II) complex, see the detailed analysis given in the Supporting Information. The ChemDraw structures are based on the single-crystal structures of similar 2:1 (Figure 3) and 1:1 complexes (Figure 2). Selective ratios of ligand/metal are shown in parentheses.

zinc(II) ions have received considerable attention as a viable platform for tracking biological zinc(II).[26,29,31,35,62,63] Our group[22a,38] and others[39−41,64] are interested in incorporating the 1,2,3-triazolyl group into the recognition component of the indicator, because, in addition to being a metal binding site, the 1,2,3-triazolyl group allows for facile CuAAC-based synthesis (hence, easy modification of the fluorophore/ionophore pair). Extending our study on multidentate 1,2,3-triazolyl-containing ligands for zinc(II),[22a,38,55] fluorescent ligands **FL14** and **FL15** were synthesized containing 7-methoxycoumarin as the fluorophore. Coumarin derivatives have been widely used in the sensing community, including sensors for zinc(II),[65−68] because of their photostability, high fluorescence quantum yields, and water solubility,[69] all of which are superior to the anthryl fluorophore in compound **1**. The *N*,*N*-di(2-picolyl)-amino ionophore is known to bind strongly with zinc(II)[57] and has been consistently utilized by the zinc(II) sensing community. The zinc(II)-dependent fluorescence of **FL14** in CH_3CN is shown in Figure S11 in the Supporting Information. A 28-fold fluorescence intensity enhancement from the free ligand (off) state to the zinc(II)-bound (on) state was observed, accompanying a minimal change in its absorption spectrum (Figure S12 in the Supporting Information). These observations are expected for indicators operating via a metal-binding-affected photoinduced electron transfer (PET) process.[70]

The interpretation that zinc(II)-coordination to **FL14** or **FL15** slows or eliminates the PET nonradiative decay process is supported by the fluorescence lifetime measurements. Because of the relevance in bioimaging, data collected from samples under pH neutral aqueous conditions are shown in Figure 7. Similar conclusions are drawn from experiments in CH_3CN. Both **FL14** and **FL15** show biexponential decays in the free ligand forms (red circles in Figures 7A and 7B). The short components (τ_1 = 0.27 ns for **FL14** and 0.13 ns for **FL15**) and long components (τ_2 = 2.4 ns for **FL14** and 2.7 ns for **FL15**) are attributed to the excited-state population (e.g., conformer) that is prone to intramolecular PET and the population that is not, respectively.[71,72] Upon formation of the zinc(II) complex, the fast components of both ligands disappear as the electron transfer process is no longer thermodynamically favorable, and only the single exponential decays of 2.7 ns for **FL14**-Zn^{2+} and 2.4 ns for **FL15**-Zn^{2+} are observed (Figures 7A and 7B, blue triangles).

Zinc(II)-dependent fluorescence enhancement of **FL14** is observed also under physiological conditions buffered by the metal chelator nitrilotriacetic acid (NTA; see Figure 8A).[73] **FL14** undergoes a 16-fold enhancement in fluorescence quantum yield upon zinc(II) binding and competes well with the NTA buffer (NTA K_d(Zn) = 14 nM). The K_d value of the **FL14**/zinc(II) complex (assuming a 1:1 stoichiometry) was determined to be 5.5 nM by plotting the fluorescence enhancement versus the "free" zinc(II) concentration.[74] An indicator with a low nanomolar K_d is appropriate for zinc(II) visualization in most biologically relevant settings, where the free zinc(II) concentration is low. The fluorescence quantum yield of **FL14**, under the simulated physiological conditions (as described in the caption of Figure 8A), is 0.04, which increases to 0.64 upon binding with zinc(II). The 16-fold enhancement

dx.doi.org/10.1021/ic302798u | *Inorg. Chem.* 2013, 52, 5838−5850

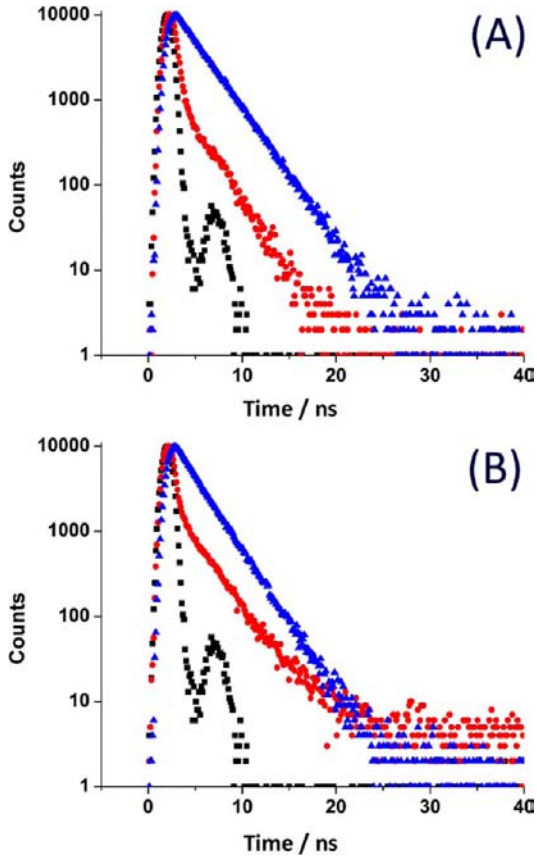

Figure 7. Fluorescence decay profiles monitored at 420 nm by exciting samples using a 370-nm nano-LED excitation source. (A) Fluorescence decay of instrument response function (IRF, black squares (■)), **FL14** (red circles (●)), and the zinc(II) complex of **FL14** (blue triangles (▲)). (B) Fluorescence decay of IRF (black squares (■)), **FL15** (red circles (●)), and the zinc(II) complex of **FL15** (blue triangles (▲)). The concentration of the indicator was 12 μM. All measurements were obtained in an aqueous NTA-HEPES buffer at pH 7.3. See details in the Supporting Information.

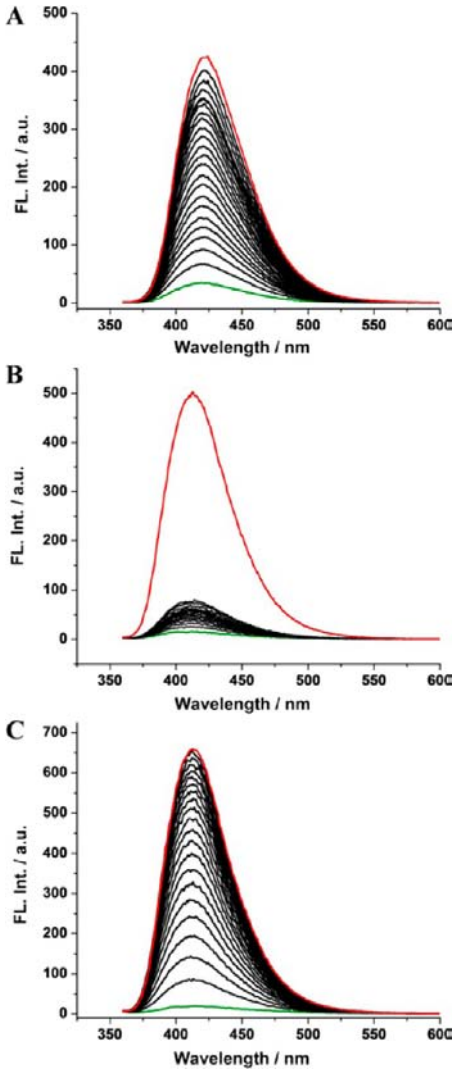

Figure 8. (A) Fluorescence spectra of **FL14** (6.6 μM, λ_{ex} = 350 nm) in the presence of $Zn(ClO_4)_2$ (0–7.2 mM) in an aqueous solution ([HEPES] = 100 mM, [NTA] = 4 mM, [KNO_3] = 100 mM, pH 7.4). (B) Fluorescence spectra of **FL15** (5.7 μM) in the presence of $Zn(ClO_4)_2$ (0–5 mM) in an aqueous solution ([HEPES] = 100 mM, [NTA] = 3 mM, [KNO_3] = 100 mM, pH 7.4). (C) Fluorescence spectra of **FL15** (5.7 μM) in the presence of $Zn(ClO_4)_2$ (0–14 mM) in an aqueous solution ([HEPES] = 100 mM, [ADA] = 8 mM, [KNO_3] = 100 mM, pH 7.4). NTA = nitrilotriacetic acid; ADA = *N*-(2-acetamido)iminodiacetic acid. The initial and final spectra of each titration experiment are coded green and red, respectively.

and the high fluorescent quantum yield of the zinc(II) complex of **FL14** are significant improvements over the previously reported compound **1**, based on anthryl fluorescence (8-fold enhancement, ϕ_{ZnL} = 0.14).[22a,38]

The fluorescence of **FL15** undergoes a 36-fold enhancement in fluorescence intensity upon the addition of increasing amounts of $Zn(ClO_4)_2$ in CH_3CN (see Figure S11 in the Supporting Information). It retains a 19-fold enhancement in fluorescence quantum yield under aqueous conditions. **FL15** has lower fluorescence quantum yields of 0.01 and 0.19 for the free ligand and zinc(II) complex, respectively, than those of **FL14**. Competition titrations of **FL15** with NTA (K_d(Zn) = 14 nM) show that the ligand is unable to compete for zinc(II) with the metal chelator (Figure 8B). **FL15** competes for binding to zinc(II) with the weaker metal chelator, *N*-(2-acetamido)-iminodiacetic acid (ADA, K_d(Zn) = 83 nM)[75] effectively (Figure 8C), thus allowing for the determination of the zinc(II) affinity of **FL15** at 90 nM (the dissociation constant of the apparent 1:1 ligand/metal complex), which is consistent with the reported zinc(II) affinity of the *N*,*N*-di(2-picolyl)amino group.[57] The affinity difference between **FL14** and **FL15** in water, in conjunction with the ITC results in CH_3CN, shows that the 1,2,3-triazolyl group strengthens the binding affinity of the ligand for zinc(II) in both organic and aqueous solvents.

The metal ion coordination preferences of both **FL14** and **FL15** generally follow the Irving–Williams series, similar to those of reported polyaza fluorescent ligands.[22a,76] The fluorescence-based selectivity data is shown in Figure S14 in the Supporting Information. As a side note and evidence of **FL14** to form complexes with other metal ions, the structures and utilities of copper(I/II) complexes of similar 1,4-isomer-containing tetradentate ligands have been reported.[5,22b,c]

The kinetics of ligand/zinc(II) binding in a pH neutral aqueous solution was investigated at 9.7 °C by employing a stopped-flow method similar to those described by Lippard and co-workers[77] and Nagano and co-workers.[78] The zinc(II) concentration was maintained at least 10 times higher than the ligand (**FL14** and **FL15**) concentration to ensure pseudo-first-order kinetics. Under these conditions, the 1:1 ligand/metal

dx.doi.org/10.1021/ic302798u | *Inorg. Chem.* 2013, 52, 5838–5850

Table 1. Summary of the Photophysical and Zinc(II)-Coordination Properties of FL14 and FL15 under pH Neutral Aqueous Conditions, and Their pK_a Values

	wavelength of maximal absorption, λ_{abs} (nm)	wavelength of maximal emission intensity, λ_{fl} (nm)	Fluorescence Quantum Yield: free ligand, ϕ_L	Fluorescence Quantum Yield: 1:1 ligand/zinc(II) complex, ϕ_{ZnL}	second-order rate constant of 1:1 ligand/zinc(II) complex formation, k_{on} (M^{-1} s^{-1})	dissociation constant of 1:1 ligand/zinc(II) complex, K_d (nM)	pK_a	Fluorescence Lifetime (ns): free ligand, τ_L[a]	Fluorescence Lifetime (ns): 1:1 ligand/zinc(II) complex, τ_{ZnL}
FL14	345	421	0.04	0.64	3.4×10^6	5.5	5.5	0.27 (82%) 2.4 (18%)	2.7
FL15	343	410	0.01	0.19	2.0×10^5	90	~3.5	0.13 (75%) 2.7 (25%)	2.4

[a]The amplitude of each component is given in parentheses.

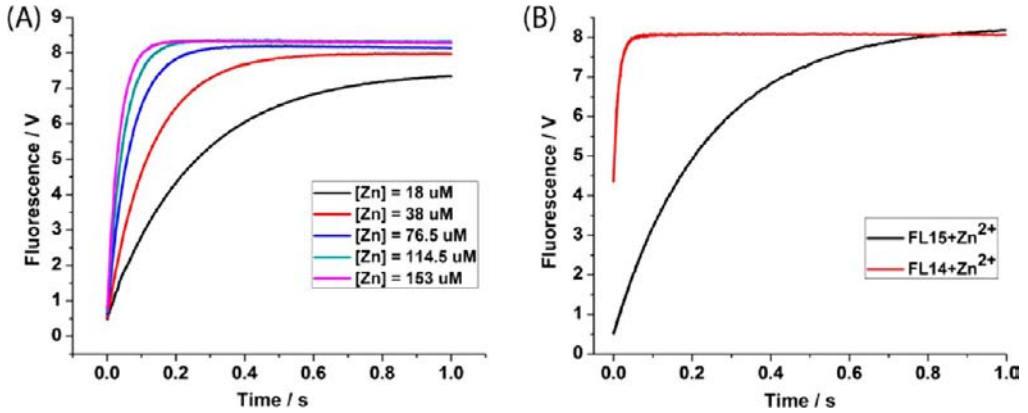

Figure 9. (A) Stopped-flow traces of **FL15** (1.0 μM) with $Zn(ClO_4)_2$ concentrations of 18, 38, 76.5, 114.5, and 153 μM at 9.7 °C in an aqueous buffer. [HEPES] = 50 mM; [KNO_3] = 100 mM; pH 7.4. The k_{obs} values are 4.0, 8.0, 15, 22, and 30 s^{-1} obtained from single exponential fits. (B) Overlaid stopped-flow traces of **FL14** and **FL15** with [Zn] = 18 μM in HEPES buffer. The k_{obs} for **FL14** is 81 s^{-1} and k_{obs} = 4.0 s^{-1} for **FL15**.

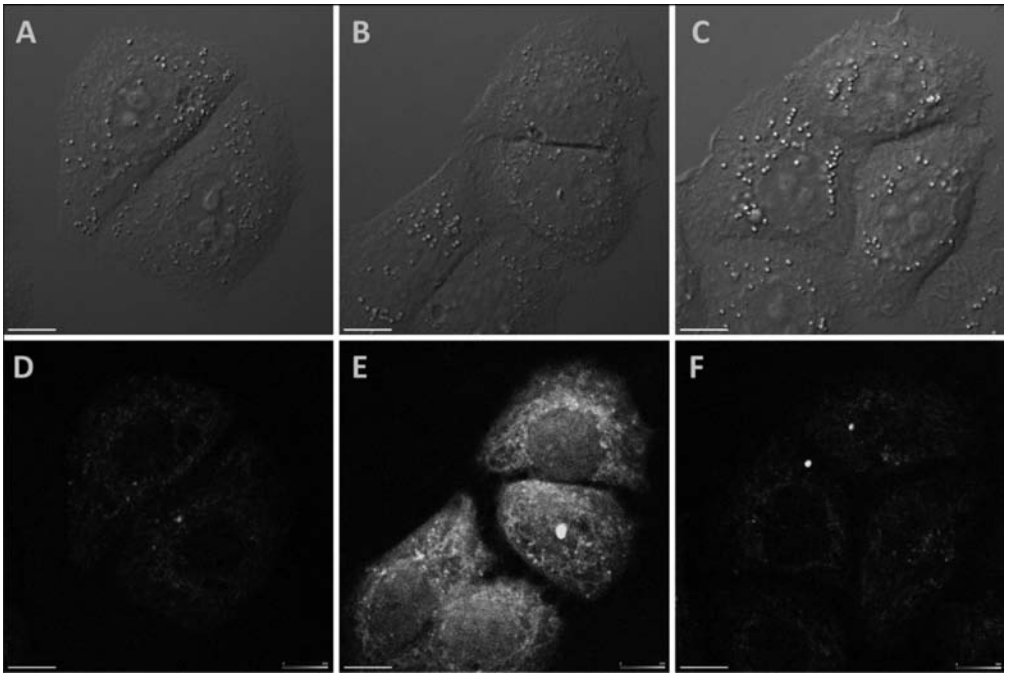

Figure 10. Images of HeLa cells incubated with **FL14** (2 μM) for 30 min. Panels (A)−(C) show differential interference contrast (DIC) images ((A) [Zn] = 0 μM, (B) [Zn] = 50 μM, and (C) [Zn] = 50 μM; [TPEN] = 50 μM), while panels (D)−(F) show the corresponding fluorescence images (λ_{ex} = 405 nm, emission window 420−520 nm). The scale bar in the lower lefthand corner in panels (D)−(F) is 10 μm; the intensity bar in the lower righthand corner in panels (D)−(F) depicts a range of 0−255.

complex presumably forms directly without the intermediacy of a 2:1 complex that was observed in the ^{1}H NMR titration experiments. At least five different zinc(II) concentrations for each ligand were used, and multiple experiments were

dx.doi.org/10.1021/ic302798u | Inorg. Chem. 2013, 52, 5838−5850

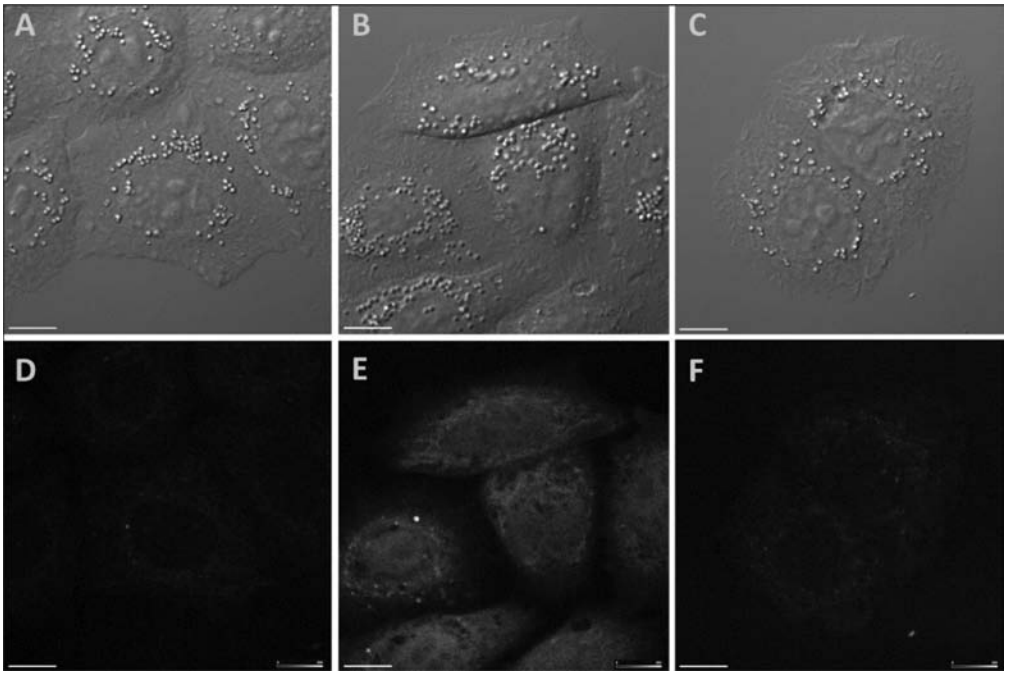

Figure 11. Images of HeLa cells incubated with **FL15** (2 μM) for 30 min. Panels (A)−(C) show differential interference contrast (DIC) images ((A) [Zn] = 0 μM, (B) [Zn] = 50 μM, and (C) [Zn] = 50 μM; [TPEN] = 50 μM)), while panels (D)−(F) show the corresponding fluorescence images (λ_{ex} = 405 nm, emission window 420−520 nm). The scale bar in the lower lefthand corner in panels (D)−(F) is 10 μm; the intensity bar in the lower righthand corner in panels (D)−(F) depicts a range of 0−255.

conducted on different days to ensure reproducibility. The experimentally determined k_{obs} (rate = k_{obs}[L]) values were plotted versus zinc(II) concentration, the slope of which yields the second-order rate constant k_{on} (k_{obs} = k_{on}[zinc(II)]; see Figure S15 in the Supporting Information). The stronger binder **FL14** also binds with zinc(II) 17 times faster than the weaker binder **FL15** (see Table 1). Figure 9A shows how the time course of the coordination reaction of **FL15** changes with respect to zinc(II) concentration. Figure 9B shows the difference in the rates of zinc(II) binding between **FL14** and **FL15** at a zinc(II) concentration of 18 μM. The k_{obs} value for **FL14** is 81 s^{-1}, while **FL15** has a lower k_{obs} of 4.0 s^{-1}, which is a 20-fold difference. The properties of **FL14** and **FL15**, with respect to zinc(II) binding under aqueous conditions, are summarized in Table 1.

Visualizing Zinc(II) Ions in Live HeLa Cells. Ligands **FL14** and **FL15** were evaluated for their potential in visualizing zinc(II) ions in live HeLa cells. All cells were incubated in a medium containing 2 μM of indicator for 30 min. The indicator-containing medium was then replaced with fresh medium that contained either basal or enriched levels of zinc(II) ions ($ZnCl_2$ was used in the experiments). The confocal microscopic images (λ_{ex} = 405 nm, Figure 10) were acquired after further incubation for 10 min; Figures 10A−C show differential interference contrast (DIC) images, and Figures 10D−F shows fluorescence images. Cells incubated with media devoid of supplemental zinc(II) afforded the images shown in Figures 10A and 10D. The fluorescence intensity of the image in Figure 10D, presumably from the emission of the free ligand and/or complex formed with pockets of endogenous zinc(II), was minimal. After incubating the cells in the presence of 50 μM $ZnCl_2$, a large increase in fluorescence was observed in the image in Figure 10E, relative to that shown in Figure 10D. Finally, the image in Figure 10F shows the reversibility of **FL14** as a zinc(II) binder under physiological conditions by adding the high-affinity zinc(II) ligand, tetrakis(2-pyridylmethyl)ethylenediamine (TPEN, pK_d(Zn) = 15.6).[79] Zinc(II) ions were sequestered by TPEN from the fluorescent zinc(II)/**FL14** complex. Consequently, the emission intensity decreased to almost the level shown in Figure 10D. Without organelle-directing functional groups, the subcellular localization of **FL14** is undefined and follows a pattern similar to that of other previously reported neutral polyaza-based indicators.[74]

Similar results were obtained with compound **FL15** (Figure 11). However, **FL15** shows the overall dimer fluorescence, relative to that of **FL14**, using the identical set of imaging parameters, which is consistent with the characterization that the fluorescence quantum yield of **FL15**/zinc(II) complex is lower than that of **FL14**. Apart from that, both indicators show potential to report intracellular [zinc(II)] changes fluorometrically under live-cell imaging conditions. There was no change of cell morphology (e.g., balling up) over the course of the microscopic experiment, indicating a minimal level of toxicity of **FL14** or **FL15** at the prescribed dosage. The fluorescence enhancement was reversed upon the addition of TPEN, corroborating that the enhanced fluorescence under zinc(II)-enriched conditions originates solely from the zinc(II)/indicator complex, rather than from any other biochemical transformations that might have given a fluorescent readout.

Visualizing Endogenous Zinc(II) in Hippocampal Slices. The effectiveness of **FL14** and **FL15** to stain zinc(II)-rich areas of live rat hippocampal slices was investigated. A commercially available zinc(II) indicator, ZP1, developed by Lippard and co-workers,[80,81] was also used, in comparison, under the same experimental conditions. The preparation of the slices and relevant experimental protocols are included in the Supporting Information. Briefly, the slices were stained via incubation in oxygenated artificial cerebrospinal fluid (aCSF) containing 10 μM of indicator for 30 min. Slices were imaged

dx.doi.org/10.1021/ic302798u | Inorg. Chem. 2013, 52, 5838−5850

using a confocal microscope equipped with a 405-nm diode laser line for exciting **FL14** and **FL15**. ZP1 requires a 488-nm excitation, which is suitable for the fluorescein fluorophore of ZP1. **FL14** resulted in clear and reproducible staining of the zinc(II)-rich dentate gyrus and CA3 regions of the hippocampus (see Figure S17 in the Supporting Information for an anatomical map), which was comparable to that of ZP1 (Figure 12). Based on physiological experiments, there is a consensus

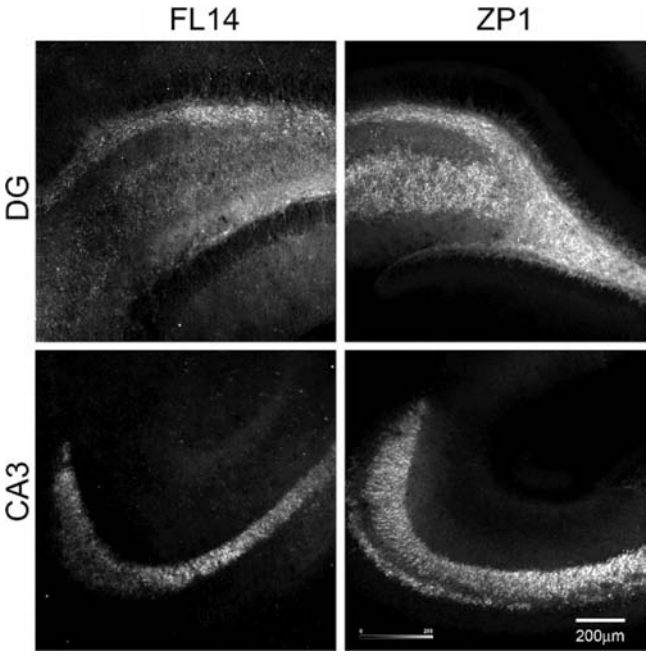

Figure 12. The indicator **FL14** stains zinc(II) in the dentate gyrus (DG) and CA3 regions of the hippocampus. Confocal microscopy images are shown, comparing live rat hippocampal slices (250 μm thick) stained with 10 μM indicators **FL14** and ZP1. Intensity bar in the lower right frame depict a range of 0−255.

that free zinc(II) ions are concentrated in the dentate gyrus and CA3 areas of the hippocampus.[82] So far, the zinc(II) staining experiments using fluorescent indicators have corroborated this conclusion.[78,83−89] **FL15**, the zinc(II) complex which has a lower fluorescence quantum yield and a higher dissociation constant than **FL14** (recall Table 1), was not effective in staining zinc(II) in the hippocampal slices (data not shown). The specificity of **FL14** for zinc(II) was confirmed using the zinc(II) chelator TPEN. Treatment of hippocampal slices with 100 μM TPEN prior to staining eliminated **FL14** fluorescence (see Figure S18 in the Supporting Information).

In our hands, ZP1 stains both the DG and CA3 regions, whereas **FL14** also stains both of those regions but with less fluorescence intensity. **FL15** does not appreciably stain either the DG or CA. The difference in zinc(II) staining between **FL14** and ZP1 may be attributed to the lower excitation energy applied in the ZP1 case (488-nm laser), which not only suppresses autofluorescence but is not attenuated as much by the optics setup of the microscope as a higher-energy 405-nm laser excitation source. Therefore, creating 1,2,3-triazolyl-integrated indicators that are excitable by lower energy lasers is our next objective.

CONCLUSION

We have compared the coordination properties of isomeric 1,2,3-triazolyl-containing ligands (e.g., **L14** and **L15**) in both solid state and solution. In the solid state, **L15** is a tridentate ligand for zinc(II) in the 1:1 ligand/metal complex, while an intermolecular 1,2,3-triazolyl coordination is maintained in the single crystals to result in a coordination polymer. The 2:1 **BrL15**/zinc(II) complex crystallizes into a *fac* stereoisomer with C_2 symmetry, which is shown to be the thermodynamically stable form in solution. The equilibrium constant of N3 1,2,3-triazolyl/CH_3CN exchange for zinc(II) binding is 18 (−1.7 kcal/mol at 298 K), as determined in an ITC experiment. This value represents the benefit of enlisting 1,2,3-triazolyl in cooperative binding to the overall zinc(II) affinity in CH_3CN. ^{1}H NMR titrations of 1,4- and 1,5-isomers with $Zn(ClO_4)_2$ reveal the structural details of the 2:1 and 1:1 ligand/zinc(II) complexes, which are corroborated by the conclusion from the single-crystal X-ray data. Competition binding experiments and stopped-flow data show that the 1,4-isomeric ligand (**FL14**) with an integrated 1,2,3-triazolyl binds stronger and faster with zinc(II) ions than the 1,5-isomer **FL15**. **FL14** and **FL15** are viable fluorescent indicators for zinc(II) ions in live-cell imaging experiments. Both indicators report a large intracellular fluorescence enhancement when zinc(II) in the growth medium is enriched, while no toxic effect was observed over the course of the staining/imaging experiments. **FL14** is capable of staining endogenous zinc(II) in the dentate gyrus and CA3 regions of rat hippocampus, which is known to accumulate free zinc(II) ions. **FL15** is ineffective due to a low affinity to zinc(II) and overall low achievable fluorescence quantum yield. Both the brightness at the excitation wavelength ($\varepsilon \times \phi_F$ = 4672 at 350 nm) and fluorescence quantum yield of the zinc(II) complex of **FL14** (ϕ_F = 0.64) are significant improvements over those previously reported for compound **1** ($\varepsilon \times \phi_F$ = 711 at 300 nm, ϕ_F = 0.14), thus achieving the objective stated in the Introduction section. The conclusion from this study shall aid in the designs of future 1,2,3-triazolyl-containing multidentate ligands.

ASSOCIATED CONTENT

Supporting Information

Procedures for syntheses, characterizations of new compounds, detailed ^{1}H NMR assignment of the 2:1 **BrL15**/zinc(II) complex, and additional spectra and images. This material is available free of charge via the Internet at http://pubs.acs.org.

AUTHOR INFORMATION

Corresponding Author

*E-mail addresses: Cathy.Levenson@med.fsu.edu (C.W.L.), davidson@magnet.fsu.edu (M.W.D.), lzhu@chem.fsu.edu (L.Z.).

Author Contributions

The manuscript was written through contributions of all authors. All authors have given approval to the final version of the manuscript.

Notes

The authors declare no competing financial interest.

ACKNOWLEDGMENTS

This work was supported by the National Institute of General Medical Sciences (NIGMS) (No. R01GM081382). The authors thank Dr. Kesavapillai Sreenath for helpful discussions

regarding the interpretation of the lifetime data, and the Institute of Molecular Biophysics (IMB) at FSU for providing access to a VP-ITC microcalorimeter (MicroCal) and an Applied Photophysics SX20 double-mixing stopped-flow apparatus. Dr. Claudius Mundoma at IMB is acknowledged for technical assistance.

REFERENCES

(1) Huisgen, R.; Szeimies, G.; Möbius, L. *Chem. Ber.* **1967**, *100*, 2494−2507.
(2) Chan, T. R.; Hilgraf, R.; Sharpless, K. B.; Fokin, V. V. *Org. Lett.* **2004**, *6*, 2853−2855.
(3) Liu, D.; Gao, W.; Dai, Q.; Zhang, X. *Org. Lett.* **2005**, *7*, 4907−4910.
(4) Detz, R. J.; Heras, S. A.; de Gelder, R.; van Leeuwen, P. W. N. M.; Hiemstra, H.; Reek, J. N. H.; van Maarseveen, J. H. *Org. Lett.* **2006**, *8*, 3227−3230.
(5) Bergbreiter, D. E.; Hamilton, P. N.; Koshti, N. M. *J. Am. Chem. Soc.* **2007**, *129*, 10666−10667.
(6) Ohmatsu, K.; Kiyokawa, M.; Ooi, T. *J. Am. Chem. Soc.* **2011**, *133*, 1307−1309.
(7) Michaels, H. A.; Zhu, L. *Chem. Asian J.* **2011**, *6*, 2825−2834.
(8) Hua, Y.; Flood, A. H. *Chem. Soc. Rev.* **2010**, *39*, 1262−1271.
(9) Lau, Y. H.; Rutledge, P. J.; Watkinson, M.; Todd, M. H. *Chem. Soc. Rev.* **2011**, *40*, 2848−2866.
(10) Kolb, H. C.; Sharpless, K. B. *Drug Discovery Today* **2003**, *8*, 1128−1137.
(11) Schweinfurth, D.; Demeshko, S.; Khusniyarov, M. M.; Dechert, S.; Gurram, V.; Buchmeiser, M. R.; Meyer, F.; Sarkar, B. *Inorg. Chem.* **2012**, *51*, 7592−7597.
(12) Guha, P. M.; Phan, H.; Kinyon, J. S.; Brotherton, W. S.; Sreenath, K.; Simmons, J. T.; Wang, Z.; Clark, R. J.; Dalal, N. S.; Shatruk, M.; Zhu, L. *Inorg. Chem.* **2012**, *51*, 3465−3477.
(13) Rostovtsev, V. V.; Green, L. G.; Fokin, V. V.; Sharpless, K. B. *Angew. Chem., Int. Ed.* **2002**, *41*, 2596−2599.
(14) Tornøe, C. W.; Christensen, C.; Meldal, M. *J. Org. Chem.* **2002**, *67*, 3057−3064.
(15) Krasiński, A.; Fokin, V. V.; Sharpless, K. B. *Org. Lett.* **2004**, *6*, 1237−1240.
(16) Zhang, L.; Chen, X.; Xue, P.; Sun, H. H. Y.; Williams, I. D.; Sharpless, K. B.; Fokin, V. V.; Jia, G. *J. Am. Chem. Soc.* **2005**, *127*, 15998−15999.
(17) Rasmussen, L. K.; Boren, B. C.; Fokin, V. V. *Org. Lett.* **2007**, *9*, 5337−5339.
(18) Kwok, S. W.; Fotsing, J. R.; Fraser, R. J.; Rodionov, V. O.; Fokin, V. V. *Org. Lett.* **2010**, *12*, 4217−4219.
(19) (a) Mindt, T. L.; Struthers, H.; Brans, L.; Anguelov, T.; Schweinsberg, C.; Maes, V.; Tourwe, D.; Schibli, R. *J. Am. Chem. Soc.* **2006**, *128*, 15096−15097. (b) Struthers, H.; Mindt, T. L.; Schibli, R. *Dalton Trans.* **2010**, *39*, 675−696.
(20) Bai, S.; Young, D. J.; Hor, T. S. A. *Chem. Asian J.* **2011**, *6*, 292−304.
(21) Crowley, J. D.; McMorran, D. A. *Top. Heterocycl. Chem.* **2012**, *28*, 31−83.
(22) (a) Huang, S.; Clark, R. J.; Zhu, L. *Org. Lett.* **2007**, *9*, 4999−5002. (b) Brotherton, W. S.; Michaels, H. A.; Simmons, J. T.; Clark, R. J.; Dalal, N. S.; Zhu, L. *Org. Lett.* **2009**, *11*, 4954−4957. (c) Rosenthal, J.; Lippard, S. J. *J. Am. Chem. Soc.* **2010**, *132*, 5536−5537.
(23) Choi, D. W.; Koh, J. Y. *Annu. Rev. Neurosci.* **1998**, *21*, 347−375.
(24) Takeda, A. *BioMetals* **2001**, *14*, 343−351.
(25) Frederickson, C. J.; Koh, J.-Y.; Bush, A. I. *Nat. Rev. Neurosci.* **2005**, *6*, 449−462.
(26) Nolan, E. M.; Lippard, S. J. *Acc. Chem. Res.* **2009**, *42*, 193−203.
(27) The brightness is calculated as the product of the extinction coefficient of a fluorophore at its excitation wavelength and its fluorescence quantum yield, ϕ_{FL}.
(28) Kimura, E.; Aoki, S. *BioMetals* **2001**, *14*, 191−204.
(29) Kikuchi, K.; Komatsu, K.; Nagano, T. *Curr. Opin. Chem. Biol.* **2004**, *8*, 182−191.
(30) Jiang, P.; Guo, Z. *Coord. Chem. Rev.* **2004**, *248*, 205−229.
(31) Lim, N. C.; Freake, H. C.; Brückner, C. *Chem.—Eur. J.* **2005**, *11*, 38−49.
(32) Thompson, R. B. *Curr. Opin. Chem. Biol.* **2005**, *9*, 526−532.
(33) Chang, C. J.; Lippard, S. J. *Met. Ions Life Sci.* **2006**, *1*, 321−370.
(34) Dai, Z.; Canary, J. W. *New J. Chem.* **2007**, *31*, 1708−1718.
(35) Carol, P.; Sreejith, S.; Ajayaghosh, A. *Chem. Asian J.* **2007**, *2*, 338−348.
(36) Tomat, E.; Lippard, S. J. *Curr. Opin. Chem. Biol.* **2010**, *14*, 225−230.
(37) Pluth, M. D.; Tomat, E.; Lippard, S. J. *Annu. Rev. Biochem.* **2011**, *0*, 333−355.
(38) Michaels, H. A.; Murphy, C. S.; Clark, R. J.; Davidson, M. W.; Zhu, L. *Inorg. Chem.* **2010**, *49*, 4278−4287.
(39) Tamanini, E.; Katewa, A.; Sedger, L. M.; Todd, M. H.; Watkinson, M. *Inorg. Chem.* **2009**, *48*, 319−324.
(40) Tamanini, E.; Flavin, K.; Motevalli, M.; Piperno, S.; Gheber, L. A.; Todd, M. H.; Watkinson, M. *Inorg. Chem.* **2010**, *49*, 3789−3800.
(41) (a) Nguyen, D. M.; Frazer, A.; Rodriguez, L.; Belfield, K. D. *Chem. Mater.* **2010**, *22*, 3472−3481. (b) Kotha, S.; Goyal, D.; Banerjee, S.; Datta, A. *Analyst* **2012**, *137*, 2871−2875.
(42) Ladbury, J. E.; Cowdhry, B. Z. In *Biocalorimetry: Applications of Calorimetry in the Biological Sciences*, 1st Edition; Wiley: Chichester, England, 1998.
(43) Boren, B. C.; Narayan, S.; Rasmussen, L. K.; Zhang, L.; Zhao, H.; Lin, Z.; Jia, G.; Fokin, V. V. *J. Am. Chem. Soc.* **2008**, *130*, 8923−8930.
(44) http://www.cambridgesoft.com/Ensemble_for_Chemistry/ChemDraw/.
(45) http://www.chem.gla.ac.uk/~louis/software/ortep3/.
(46) Glerup, J.; Goodson, P. A.; Hodgson, D. J.; Michelsen, K.; Nielsen, K. M.; Weihe, H. *Inorg. Chem.* **1992**, *31*, 4611−4616.
(47) Banthia, S.; Samanta, A. *Eur. J. Org. Chem.* **2005**, *2005*, 4967−4970.
(48) Maity, B.; Gadadhar, S.; Goswami, T. K.; Karande, A. A.; Chakravarty, A. R. *Dalton Trans.* **2011**, *40*, 11904−11913.
(49) Mikata, Y.; Fujimoto, T.; Fujiwara, T.; Kondo, S. *Inorg. Chim. Acta* **2011**, *370*, 420−426.
(50) Dobrawa, R.; Lysetska, M.; Ballester, P.; Grüne, M.; Würthner, F. *Macromolecules* **2005**, *38*, 1315−1325.
(51) Shunmugam, R.; Gabriel, G.; Smith, C.; Aamer, K.; Tew, G. *Chem.—Eur. J.* **2008**, *14*, 3904−3907.
(52) Zhang, L.; Zhu, L. *J. Org. Chem.* **2008**, *73*, 8321−8330.
(53) Younes, A. H.; Zhang, L.; Clark, R. J.; Zhu, L. *J. Org. Chem.* **2009**, *74*, 8761−8772.
(54) Kano, K.; Kondo, M.; Inoue, H.; Kitagishi, H.; Colasson, B.; Reinaud, O. *Inorg. Chem.* **2011**, *50*, 6353−6360.
(55) Younes, A. H.; Clark, R. J.; Zhu, L. *Supramol. Chem.* **2012**, *24*, 696−706.
(56) Sessler, J. L.; Gross, D. E.; Cho, W.; Lynch, V. M.; Schmidtchen, F. P.; Bates, G. W.; Light, M. E.; Gale, P. A. *J. Am. Chem. Soc.* **2006**, *128*, 12281−12288.
(57) Anderegg, G.; Hubmann, E.; Podder, N. G.; Wenk, F. *Helv. Chim. Acta* **1977**, *60*, 123−140.
(58) This is the reverse titration of the ITC experiments.
(59) The argument here is that the ring flip of the 5-membered coordination rings, which leads to the exchange of pseudo-equatorial and pseudo-axial methylene protons (i.e., H_e and H_f), is facilitated by the cleavage and reformation of the coordinative N−Zn bonds. Therefore, the observation of an AB system of H_e in the 1:1 complex suggests that the pyridyl-Zn coordination equilibrium is slower than the NMR time scale, while a singlet of H_f is consistent with a 1,2,3-triazolyl-Zn coordination kinetics faster than the ^{1}H NMR time scale. Similar observations were recorded in ref 22a.
(60) de Silva, A. P.; Moody, T. S.; Wright, G. D. *Analyst* **2009**, *134*, 2385−2393.

(61) Xu, Z.; Yoon, J.; Spring, D. R. *Chem. Soc. Rev.* **2010**, *39*, 1996−2006.
(62) Callan, J. F.; de Silva, A. P.; Magri, D. C. *Tetrahedron* **2005**, *61*, 8551−8588.
(63) Terai, T.; Nagano, T. *Curr. Opin. Chem. Biol.* **2008**, *12*, 515−521.
(64) Jobe, K.; Brennan, C. H.; Motevalli, M.; Goldup, S. M.; Watkinson, M. *Chem. Commun.* **2011**, *47*, 6036−6038.
(65) Lim, N. C.; Yao, L.; Freake, H. C.; Brückner, C. *Bioorg. Med. Chem. Lett.* **2003**, *13*, 2251−2254.
(66) Lim, N. C.; Bruckner, C. *Chem. Commun.* **2004**, *9*, 1094−1095.
(67) Lim, N. C.; Schuster, J. V.; Porto, M. C.; Tanudra, M. A.; Yao, L.; Freake, H. C.; Brückner, C. *Inorg. Chem.* **2005**, *44*, 2018−2030.
(68) Zhang, L.; Dong, S.; Zhu, L. *Chem. Commun.* **2007**, 1891−1893.
(69) Li, H.; Cai, L.; Chen, Z. Coumarin-Derived Fluorescent Chemosensors. In *Advances in Chemical Sensors*; Wang, W., Ed.; InTech: Shanghai, PRC, 2012; p 121. (ISBN: 9783077925.)
(70) Zhu, L.; Zhang, L.; Younes, A. H. *Supramol. Chem.* **2009**, *21*, 268−283.
(71) Thiagarajan, V.; Selvaraju, C.; Malar, E. J. P.; Ramamurthy, P. *ChemPhysChem* **2004**, *5*, 1200−1209.
(72) (a) Zhang, R.; Wang, Z.; Wu, Y.; Fu, H.; Yao, J. *Org. Lett.* **2008**, *10*, 3065−3068. (b) Ajayakumar, G.; Godipas, K. R. *Photochem. Photobiol. Sci.* **2008**, *7*, 826−833.
(73) Patton, C.; Thompson, S.; Epel, D. *Cell Calcium* **2004**, *35*, 427−431.
(74) (a) Zhang, L.; Murphy, C. S.; Kuang, G.-C.; Hazelwood, K. L.; Constantino, M. H.; Davidson, M. W.; Zhu, L. *Chem. Commun.* **2009**, 7408−7410. (b) Kuang, G.; Allen, J. R.; Baird, M. A.; Nguyen, B. T.; Zhang, L.; Morgan, T. J.; Levenson, C. W.; Davidson, M. W.; Zhu, L. *Inorg. Chem.* **2011**, *50*, 10493−10504.
(75) http://www.stanford.edu/~cpatton/webmaxc/webmaxcS.htm.
(76) Sreenath, K.; Allen, J. R.; Davidson, M. W.; Zhu, L. *Chem. Commun.* **2011**, *47*, 11730−11732.
(77) Nolan, E. M.; Jaworski, J.; Okamoto, K.; Hayashi, Y.; Sheng, M.; Lippard, S. J. *J. Am. Chem. Soc.* **2005**, *127*, 16812−16823.
(78) Komatsu, K.; Kikuchi, K.; Kojima, H.; Urano, Y.; Nagano, T. *J. Am. Chem. Soc.* **2005**, *127*, 10197−10204.
(79) Rana, U.; Kothinti, R.; Meeusen, J.; Tabatabai, N. M.; Krezoski, S.; Petering, D. H. *J. Inorg. Biochem.* **2008**, *102*, 489−499.
(80) Walkup, G. K.; Burdette, S. C.; Lippard, S. J.; Tsien, R. Y. *J. Am. Chem. Soc.* **2000**, *122*, 5644−5645.
(81) Burdette, S. C.; Walkup, G. K.; Spingler, B.; Tsien, R. Y.; Lippard, S. J. *J. Am. Chem. Soc.* **2001**, *123*, 7831−7841.
(82) Ketterman, J. K.; Li, Y. V. *J. Neurosci. Res.* **2008**, *86*, 422−434.
(83) Burdette, S. C.; Frederickson, C. J.; Bu, W.; Lippard, S. J. *J. Am. Chem. Soc.* **2003**, *125*, 1778−1787.
(84) Woodroofe, C. C.; Masalha, R.; Barnes, K. R.; Frederickson, C. J.; Lippard, S. J. *Chem. Biol.* **2004**, *11*, 1659−1666.
(85) Chang, C. J.; Nolan, E. M.; Jaworski, J.; Okamoto, K.; Hayashi, Y.; Sheng, M.; Lippard, S. J. *Inorg. Chem.* **2004**, *43*, 6774−6779.
(86) Komatsu, K.; Urano, Y.; Kojima, H.; Nagano, T. *J. Am. Chem. Soc.* **2007**, *129*, 13447−13454.
(87) Kim, H.; Seo, M.; An, M.; Hong, J.; Tian, Y.; Choi, J.; Kwon, O.; Lee, K.; Cho, B. *Angew. Chem., Int. Ed.* **2008**, *47*, 5167−5170.
(88) Masanta, G.; Lim, C. S.; Kim, H. J.; Han, J. H.; Kim, H. M.; Cho, B. R. *J. Am. Chem. Soc.* **2011**, *133*, 5698−5700.
(89) Mei, Y.; Frederickson, C. J.; Giblin, L. J.; Weiss, J. H.; Medvedeva, Y.; Bentley, P. A. *Chem. Commun.* **2011**, *47*, 7107−7109.